IEEE Access
Multidisciplinary ⋮ Rapid Review ⋮ Open Access Journal

Received January 10, 2022, accepted January 29, 2022, date of publication February 7, 2022, date of current version February 16, 2022.

Digital Object Identifier 10.1109/ACCESS.2022.3149915

Performance Analysis for AOA-Based Localization Under Millimeter-Wave Wireless Networks

JIAJUN HE, (Student Member, IEEE), AND YOUNG JIN CHUN, (Member, IEEE)
Department of Electrical Engineering, City University of Hong Kong, Hong Kong, SAR, China

Corresponding author: Young Jin Chun (yjchun@cityu.edu.hk)

This work was supported in part by the Early Career Scheme under Project 9048208 established under the University Grant Committee (UGC) of the Hong Kong Special Administrative Region (HKSAR), China; in part by the City University of Hong Kong (CityU), Startup Grant 7200618; in part by the CityU, Strategic Research Grant 7005467; and in part by the RMGS Donation Grant 9229080.

ABSTRACT Millimeter-Wave (mmWave) communication is a promising solution for achieving high data rate and low latency in 5G wireless networks. Since directional beamforming and antenna arrays are exploited in the mmWave networks, accurate angle-of-arrival (AOA) measurements can be obtained and utilized for localization purposes. In this work, we consider the AOA-based positioning for the mmWave networks using stochastic geometry and analyze how the Cramér-Rao lower bound (CRLB) is affected by the spatial distribution of nodes, including the target and participating anchors. In order to apply the CRLB on a network setting with random node locations, we propose an accurate approximation of the CRLB using the $\lceil L/4 \rceil$-th value of the ordered distances where L is the number of participating anchors. These findings provide us deep insight into optimum network design that meets specified localization requirements.

INDEX TERMS Millimeter-wave, angle-of-arrival, localizability, Cramér-Rao lower bound.

I. INTRODUCTION

Positioning techniques received considerable attention due to the emergency of internet-of-things, which can be utilized to ameliorate the user experience of location-based services, including indoor navigation, asset tracking, and simultaneous localization and mapping (SLAM) [1]–[3]. In the 5G wireless networks, accurate angle-of-arrival (AOA) information can be obtained by leveraging the massive antenna array and highly directional transmission [4]. Thus, AOA-based localization is regarded as a promising candidate to achieve high-precision localization for 5G networks.

A. MOTIVATION

Millimeter-Wave (mmWave) is a promising technology for 5G wireless networks to meet the requirements of large bandwidth and high carrier frequency [5]. Due to its high transmission rate, mmWave signals enable us to efficiently detect and resolve the multipath components, which provide us an opportunity to achieve submeter level localization accuracy [6], [7]. However, the coverage area of the mmWave signals is limited due to its fast attenuation. Blockage and multipath effects also take significant roles in the mmWave signal propagation, greatly increasing localization error [8]. In addition, the cost of the mmWave-based system is exorbitant due to the deployment of the massive antenna array and a large number of mmWave anchors. The experimental verification for the mmWave-based system is complicated and time-consuming, which brings challenges to examining the localization performance for the mmWave-based system.

Motivated by these limitations, we attempt to provide an analytical tool to quantify the localization performance for the AOA-based positioning and examine how its performance is affected by the mmWave channel over diverse channel propagation conditions. To characterize the fundamental limits of the mmWave-based localization system, Cramér-Rao lower bound (CRLB) is applied, which indicates the optimal localization performance for any unbiased estimator. However, the CRLB is generally assessed by given specified anchor geometry, which cannot reflect how the random network configurations affect this metric. Thus, stochastic geometry is applied to allow random spatial node locations, including the target and anchor locations. Based on our devised result, the system designers can examine how different network parameters and the overall setup influence localization performance without prolix and complicated experimental verification.

B. RELATED WORK

Localization based on the mmWave signals is thoroughly investigated in the existed literature. Based on the processing

The associate editor coordinating the review of this manuscript and approving it for publication was Qinghua Guo.

methods, mmWave based localization can be categorized into proximity, fingerprinting, and geometry-based [9]. A single-anchor localization method for mmWave wireless networks is presented in [10], which leverages time delay and angle information to locate the target of interest. In [11], the authors utilized the received signal strength (RSS)-based fingerprinting algorithm to estimate the target location using commercial mmWave Wi-Fi. Due to the fast attenuation of mmWave signals, the localization performance under mmWave networks is subject to none-line-of-sight (NLOS) components, and the impact of the NLOS propagation is introduced in [12]. Furthermore, a neural networks-enhanced hybrid localization framework for the mmWave wireless networks is proposed in [13] to achieve high-precision localization purposes.

To quantify the localization error, L-localizability and CRLB are utilized to analyze the performance of AOA-based positioning. The L-localizability is first introduced in [14] to identify whether a target is *localizable* with a sufficient number of participating anchors. In [14], the authors modeled a cellular network with a homogeneous Poisson point process (HPPP) and applied a *dominant interferer analysis* to derive an expression for L-localizability. With an emphasis on mmWave networks, a reflection hyperbola model is proposed in [15] to analyze the target localizability, where the authors considered how the first-order reflection path affects this metric. Considering the CRLB, a performance benchmark is provided to quantify localization performance for the mmWave-based positioning system [16]. The impacts of the massive antenna array and multipath propagation on the CRLB under mmWave wireless network are examined in [17]. However, these works assumed that the locations of the target and anchors are fixed. To examine the localization performance with random network settings, the authors of [18] derived an accurate approximation for the time-of-arrival (TOA)-based CRLB by utilizing the second-largest inter-nodal angle, which introduced a new paradigm to analyze the localization performance in the area of stochastic geometry. For RSS-based localization, [19] applied u-statistics to approximate CRLB, which is only accurate when numerous anchors participate in the localization procedure. In contrast to TOA/RSS-based localization, a comprehensive analysis of AOA-based localization using stochastic geometry cannot be found in the open literature, which motivates us to extend the CRLB paradigm in [18] to the AOA-based positioning.

C. CONTRIBUTION

We aim to exploit the localization error in a random mmWave network using stochastic geometry and provide insight into how the network parameters affect the localization performance. The stochastic geometric framework in [18] is applied to analyze the impact of random anchor placement on CRLB. The main challenges of this paper are how to utilize a single random variable to approximate the AOA-based CRLB and how to bridge the gap between this metric and mmWave channels. In addition, the NLOS propagation takes a significant role in the mmWave signal transmission. Thus, a suitable mmWave model is required to analyze how the NLOS effect influences the localization performance. The main contributions of this paper are listed as follows:

1) L-LOCALIZABILITY

A tractable expression of L-localizability is derived for the mmWave networks, where the directional antenna, Nakagami fading, and the NLOS effect's impacts on mmWave-based localization systems are assessed. An asymptotic bound for the distribution of the L-localizability is provided to track the performance of AOA-based localization under mmWave networks. Thus, the system designers can have insight into how to optimize the network environment to improve the localization performance.

2) DISTRIBUTION OF AOA-BASED CRLB

In [18], the authors applied stochastic geometry to TOA-based localization, which open a new paradigm to evaluate the localization performance under random wireless networks. To the best of our knowledge, there is no prior work that investigates the impact of random geometry on AOA-based localization. Motivated by [18], we accurately approximate the AOA-based CRLB using the $\lceil L/4 \rceil$-th ordered distance, and merge the impacts of mmWave channels into the devised result. The obtained distribution provides an average performance bound for the system designers how to achieve the stated localization requirements by selecting the most appropriate network parameters.

The rest of this paper is organized as follows. The system model is presented in Section II, localization performances are analyzed in Section III, and numerical results are provided in Section IV. Finally, Section V concludes the paper.

II. SYSTEM MODEL

In this section, we present the underlying model for analysis.

A. NETWORK MODEL

We consider downlink transmission in a mmWave network where the locations of anchors follow an HPPP[1] with anchor density λ. Let us denote the locations of the anchors as $\boldsymbol{\psi} = [x, y] \in \mathbb{R}^2$, and the distance between an arbitrary anchor and target as $r = ||\boldsymbol{\psi}||$, where $\|\cdot\|$ is the Euclidean norm. Since the channel gains of NLOS paths are typically weaker than those from the line-of-sight (LOS) [23], we make the following assumption.

Assumption 1: The LOS region of the target can be approximated by a LOS ball $b(O, r_L)$, which only contains the LOS anchors. The anchors outside the LOS ball may be a LOS anchor or a NLOS anchor with a certain probability.[2]

Remark 1: The number of anchors inside the LOS ball, i.e., L, is also regraded as the average number of anchor the target

[1] HPPP has been widely leveraged to various network models, such as cellular networks and wireless sensor networks, due to its tractability [20]–[22].

[2] This assumption is widely applied and validated in the existed literature [23]–[26].

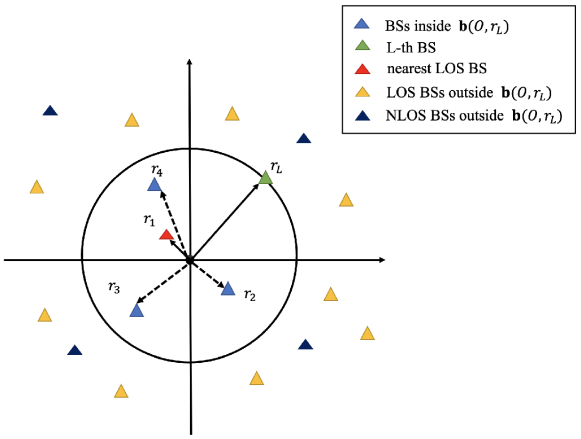

FIGURE 1. System model of mmWave wireless network.

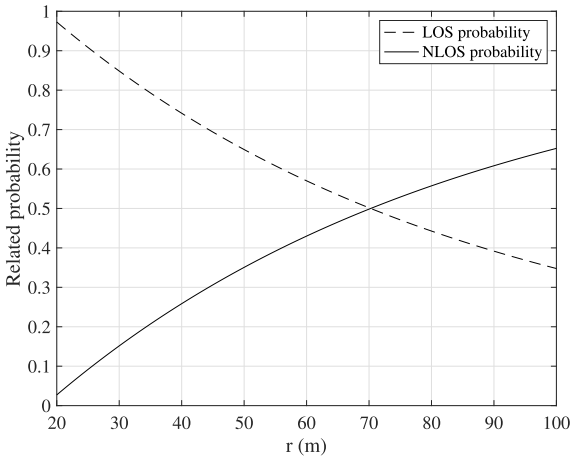

FIGURE 2. The LOS and NLOS probability in mmWave wireless networks.

can be observed. Conditioned on the number of participating anchors, coverage area of the LOS ball can be computed based on the Theorem 2 from [26].

As illustrated in Fig. 1, we assume that the target is located at the origin O and the anchors are randomly distributed in the $\mathbb{R}^2$ plane. Given that L anchors participate on the localization, we will denote the nearest and furthest distances between the associated anchor and target in the LOS ball as r_1 and r_L, respectively. Based on the model, the distance distribution of the anchors residing in the localization ball is given by [27]

$$f_{r|r_1,r_L}(r) = \frac{2r}{r_L^2 - r_1^2}, \tag{1}$$

where r is an unordered parameter with $r_1 \leq r \leq r_L$. With the particular interest of the distribution of l-th nearest anchor, we sort the distance between the anchor and target in an ascending order. Consequently, the probability density function (PDF) and cumulative distribution function (CDF) of the l-th nearest anchor are given by [28]:

$$\begin{aligned} f_{r_l}(r_l) &= \frac{2(\lambda\pi r_l^2)^l}{r_l(l-1)!}e^{-\lambda\pi r_l^2}, \\ F_{r_l}(r_l) &= 1 - \sum_{n=0}^{l-1}\frac{1}{n!}e^{-2\pi\lambda r_l^2}(2\pi\lambda r_l^2)^n, \end{aligned} \tag{2}$$

where r_l is an ordered parameter with $1 \leq l \leq L$.

B. CHANNEL MODEL

We consider a widely adopted mmWave channel model, where the probability of the associated anchor to be a LOS transmitter, referred to as *LOS probability*, is given by [29]

$$P_{LOS}(r) = \min\left(\frac{A}{r}, 1\right)\left(1 - e^{-\frac{r}{B}}\right) + e^{-\frac{r}{B}}, \tag{3}$$

where r is the link distance between the target and the anchor, the NLOS probability is $P_{NLOS}(r) = 1 - P_{LOS}(r)$, $A = 18$m and $B = 63$m for urban environment.

Remark 2: In Fig. 2, we plot the LOS/NLOS probability across different link distances. It is evident that as the link distance between the target and anchor increases, the corresponding anchor is more likely to be a NLOS transmitter. It indicates that the signal transmitted over a long-distance is more susceptible to blockage and multi-path effects. Furthermore, we can observe that P_{LOS} is close to 1 when the distance r is less than 20m, which justifies Assumption 1.

The target has a single antenna, whereas each anchor is equipped with a directional antenna array with N_t elements and all anchors transmit with a constant power P_t. We use a subscript q to denote LOS/NLOS link, *i.e.*, $q = \{L, N\}$ for LOS and NLOS link, respectively.[3] The received signal power from the l-th anchor is given by $N_t G_T h_l r_l^{\alpha_q}$, where G_T is the antenna gain at the anchor, h_l is the small-scale fading gain that follows a Gamma distribution, *i.e.*, $h_l \sim \Gamma(M_q, \frac{1}{M_q})$ with parameter M_q, and α_q denote the path-loss exponent; α_L for the LOS link and α_N for the NLOS link, respectively. The antenna gain G_T is modeled by the flat-top antenna radiation pattern as follows [30]

$$G_T = \begin{cases} G_1 & \text{for main lobe with prob. } p_1 = \dfrac{\varphi}{2\pi}, \\ G_2 & \text{for side lobe with prob. } p_2 = 1 - p_1. \end{cases} \tag{4}$$

C. AOA MEASUREMENT

Let us denote the AOA between the l-th anchor θ_l and the location of target $\boldsymbol{\psi}_t = [x_t, y_t]$ as

$$\tan(\theta_l) = \frac{y_l - y_t}{x_l - x_t}, \quad l = 1, \ldots, L, \tag{5}$$

where we used subscript t and l to indicate the target and the l-th anchor, respectively. The AOA measurement at l-th anchor is modeled by

$$\begin{aligned} r_{AOA,l} &= \theta_l + n_{AOA,l} \\ &= \tan^{-1}\left(\frac{y_l - y_t}{x_l - x_t}\right) + n_{AOA,l}, \end{aligned} \tag{6}$$

where $n_{AOA,l}$ imitates the measurement error with variance $\sigma^2_{AOA,l}$. The vector representation of the AOA measurements

[3]We assume that there is no correlation between the LOS link and NLOS link, *i.e.,* the LOS link and NLOS are independent [29].

is given by

$$\boldsymbol{r}_{AOA} = \boldsymbol{f}_{AOA}(\boldsymbol{\psi}_t) + \boldsymbol{n}_{AOA,l}, \tag{7}$$

where $\boldsymbol{r}_{AOA}$, $\boldsymbol{n}_{AOA}$, and $\boldsymbol{f}_{AOA}(\boldsymbol{\psi}_t)$ are respectively defined by

$$\begin{aligned}
\boldsymbol{r}_{AOA} &= \left[r_{AOA,1}, r_{AOA,2}, \ldots, r_{AOA,L}\right]^T, \\
\boldsymbol{f}_{AOA}(\boldsymbol{\psi}_t) &= \left[\theta_1, \theta_2, \ldots, \theta_L\right]^T, \\
\theta_l &= \tan^{-1}\left(\frac{y_l - y_t}{x_l - x_t}\right), \\
\boldsymbol{n}_{AOA} &= \left[n_{AOA,1}, n_{AOA,2}, \ldots, n_{AOA,L}\right]^T.
\end{aligned} \tag{8}$$

III. PERFORMANCE ANALYSIS

In this section, we characterize the L-localizability and CRLB of AOA-based localization for mmWave networks.

A. L-LOCALIZABILITY

L-localizability was first introduced in [14], which is defined as the probability of having at least L participating anchors in the localization procedure. We assume that the associated anchor can align the beam by the implementation of sophisticated beam training protocols [31]. The received signal-to-interference-plus-noise ratio (SINR) at the target from the L-th anchors located in the LOS ball can be expressed as

$$SINR_L = \frac{G_1 h_L r_L^{-\alpha_L}}{\sigma_n^2 + I}, \tag{9}$$

where $\sigma_n^2 = \frac{\sigma_t^2}{\beta P_t N_t}$ is the normalized noise power, σ_t^2 is the thermal noise power, $\beta = \left(\frac{\lambda_w}{4\pi}\right)^2$ is the path-loss intercept with antenna wavelength, λ_w, and I is the aggregate interference. In [14], the L-localizability is defined for a given SINR threshold τ as

$$P_L(\tau) = P(SINR_L \geq \tau). \tag{10}$$

The aggregate interference I in (9) consist of two components; I_{in} and I_{out}, which is the interference from the nodes inside and outside the LOS ball respectively. Then we have

$$\begin{aligned}
I &= I_{in} + I_{out} \\
&= \sum_{i=1, i\neq L}^{L-1} a_i G_T h_i r_i^{-\alpha_L} + \sum_{j=L+1}^{\infty} b_j G_T h_j r_j^{-\alpha_q},
\end{aligned} \tag{11}$$

where the indicators $a_i, b_j \in \{0, 1\}$ represent the network load, the probability $P(a_i = 1) = q$, $P(b_j = 1) = p$ correspond to the anchor activation probability, and the indicators a_i, b_j are fixed throughout the localization procedure. To simplify the derivation, we will express the interference inside the LOS ball as follows

$$I_{in} = G_T h_1 r_1^{-\alpha_L} + \sum_{i=2}^{L-1} a_i G_T h_i r_i^{-\alpha_L}. \tag{12}$$

Let us denote $I_1 \triangleq G_T h_1 r_1^{-\alpha_L}$ and $\hat{I}_{in} \triangleq \sum_{i=2}^{L-1} a_i G_T h_i r_i^{-\alpha_L}$. Based on the dominant interference analysis [14], I_1 and $\hat{I}_{in}$ can be approximated by the following Lemma.

Lemma 1: *I_1 and $\hat{I}_{in}$ can be approximated by its mean*

$$\begin{aligned}
\hat{I}_{in} &\approx \mathbb{E}\left[\hat{I_{in}} | r_1, r_L, L\right] \\
&= \mathbb{E}[G_T] \cdot \mathbb{E}[h] \cdot \frac{2(\hat{L} - 1)}{2 - \alpha_L} \cdot \frac{r_L^{2-\alpha_L} - r_1^{2-\alpha_L}}{r_L^2 - r_1^2}, \\
I_1 &\approx \mathbb{E}\left[I_1 | r_1\right] = \mathbb{E}[G_T] \cdot \mathbb{E}[h] \cdot r_1^{-\alpha_L},
\end{aligned} \tag{13}$$

where $\hat{L}$ is the number of active anchors inside the LOS ball, $\mathbb{E}[G_T] = G_1 p_1 + G_2 p_2$, and $\mathbb{E}[h]$ is the mean channel gain. Note that (13) are functions of r_1 and r_L.

Proof: See Appendix A. □

Based on the Lemma 1, the denominator of $SINR_L$ can be expressed as

$$\begin{aligned}
I + \sigma_n^2 &\overset{(a)}{=} I_{in} + I_{out} + \sigma_n^2 \\
&\overset{(b)}{=} I_1 + \hat{I}_{in} + I_{out} + \sigma_n^2 \\
&\overset{(c)}{=} I_{out} + \sigma^2,
\end{aligned} \tag{14}$$

where step (a) follows from (11), step (b) follows from (12), and we substitute $\sigma^2 = I_1 + \hat{I}_{in} + \sigma_n^2$ in step (c). Based on Assumption 1, I_{out} consists of interference generated by both LOS or NLOS anchors as expressed below [23]–[26]

$$I_{out} = I_L + I_N, \tag{15}$$

where I_L and I_N represents the interference generated by the LOS and NLOS anchors, respectively, that are located outside the LOS ball. Then the Laplace transform of I_{out} is

$$\begin{aligned}
\mathcal{L}_{I_{out}}(s) &= \mathcal{L}_{I_L}(s)\mathcal{L}_{I_N}(s) = \mathbb{E}_{I_L}\left[e^{-sI_L}\right]\mathbb{E}_{I_N}\left[e^{-sI_N}\right] \\
&= \exp\left(-2\pi\lambda p \cdot \omega\left(s | r_L, \alpha_q\right)\right),
\end{aligned} \tag{16}$$

where $\omega\left(s | r_L, \alpha_q\right)$ is defined below

$$\begin{aligned}
&\omega\left(s | r_L, \alpha_q\right) \\
&\triangleq P_{LOS}(r) \int_{r_L}^{\infty} \left(1 - \mathbb{E}_{h,G_T}\left[e^{-shG_T r^{-\alpha_L}}\right]\right) rdr \\
&\quad + P_{NLOS}(r) \int_{r_L}^{\infty} \left(1 - \mathbb{E}_{h,G_T}\left[e^{-shG_T r^{-\alpha_N}}\right]\right) rdr.
\end{aligned} \tag{17}$$

The term $\mathbb{E}_{h,G_T}[\exp(-shG_T r^{\alpha_q})]$ is derived as follows

$$\begin{aligned}
&\mathbb{E}_{h,G_T}[\exp\left(-shG_T\ r^{\alpha_q}\right)] \\
&\overset{(a)}{=} p_1\ \mathbb{E}_h[e^{-shG_1\ r^{\alpha_q}}] + p_2\ \mathbb{E}_h[e^{-shG_2\ r^{\alpha_q}}] \\
&\overset{(b)}{=} \frac{p_1}{(1 + sG_1 \cdot r^{-\alpha_q})^{M_q}} + \frac{p_2}{(1 + sG_2 \cdot r^{-\alpha_q})^{M_q}},
\end{aligned} \tag{18}$$

where we applied (4) in step (a) and utilized the Laplace transform of the Gamma random variable in step (b) [29]. To conclude, the L-localizability in (10) can be evaluated as

$$\begin{aligned}
P_L(\tau) &\overset{(a)}{=} \sum_{i=1}^{M_L} (-1)^{i+1} \binom{M_L}{i} \mathbb{E}\left[e^{-\frac{i\tau\eta\left(\sigma^2 + I_{out}\right) r_L^{\alpha_L}}{G_1}}\right] \\
&\overset{(b)}{=} \sum_{i=1}^{M_L} (-1)^{i+1} \binom{M_L}{i} \mathbb{E}_{r_1, r_L}
\end{aligned}$$

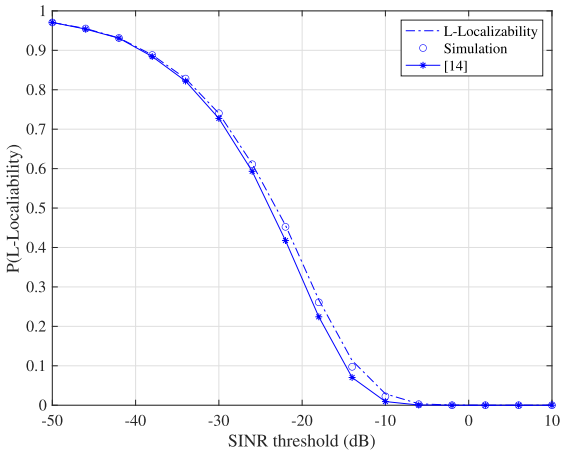

FIGURE 3. Accuracy of *L*-localizability.

$$\times \left[e^{-i\tau\mu\sigma^2} \cdot \mathbb{E}_{I_{out}} \left(e^{-i\tau\mu I_{out}} \right) \right]$$
$$\overset{(c)}{=} \sum_{i=1}^{M_L} (-1)^{i+1} \binom{M_L}{i} \int_0^{\infty} \int_0^{r_L} e^{-i\tau\mu\sigma^2} \mathcal{L}_{I_{out}}(i\tau\mu) \times f_{r_1}(\iota) f_{r_L}(\upsilon) d\iota d\upsilon, \quad (19)$$

where $\eta = M_L(M_L!)^{-\frac{1}{M_L}}$, (14) and Alzer's inequality [32] are used in step (a), a change of variable is used in step (b), *i.e.*, $\mu = \frac{\eta r_L^{\alpha}}{G_1}$, and $\mathbb{E}_{I_{out}}\left[e^{-i\tau\mu I_{out}}\right] = \mathcal{L}_{I_{out}}(i\tau\mu)$ in step (c). Note that $\mathcal{L}_{I_{out}}(s)$ in (16) is a function of r_L, whereas $\sigma^2 = I_1 + \hat{I}_{in} + \sigma_n^2$ is a function of both r_1 and r_L.

Remark 3: When the parameter M_L is equal to 1, (19) provides the localization performance for Rayleigh fading. Different from the approximation method in [14], we only approximate the interference inside the LOS ball by its mean value. We can observe in Fig. 3 that our devised method is slightly better than that in [14].

B. APPROXIMATION OF CRAMER-RAO LOWER BOUND

We derive the AOA-based random CRLB using the FIM, denoted by $\boldsymbol{I}_{AOA}(\boldsymbol{\psi}_t)$, as [9]

$$\boldsymbol{I}_{AOA}(\boldsymbol{\psi}_t) = \left(\frac{\partial \boldsymbol{f}_{AOA}(\boldsymbol{\psi}_t)}{\partial \boldsymbol{\psi}_t} \right)^T \cdot \boldsymbol{C}_{AOA}^{-1} \cdot \frac{\partial \boldsymbol{f}_{AOA}(\boldsymbol{\psi}_t)}{\partial \boldsymbol{\psi}_t}$$
$$= \begin{bmatrix} \sum_{i=1}^{L} \frac{(y_t - y_i)^2}{r_i^4 \cdot \sigma_{AOA,i}^2} & -\sum_{i=1}^{L} \frac{(x_t - x_i)(y_t - y_i)}{r_i^4 \cdot \sigma_{AOA,i}^2} \\ -\sum_{i=1}^{L} \frac{(x_t - x_i)(y_t - y_i)}{r_i^4 \cdot \sigma_{AOA,i}^2} & \sum_{i=1}^{L} \frac{(x_t - x_i)^2}{r_i^4 \cdot \sigma_{AOA,i}^2} \end{bmatrix}, \quad (20)$$

where $\boldsymbol{C}_{AOA}$ represents the noise covariance matrix and $\boldsymbol{f}_{AOA}(\boldsymbol{\psi}_t)$ is the angle vector with respect to $\boldsymbol{\psi}_t$, given by

$$\boldsymbol{C}_{AOA} = \text{diag}\left(\sigma_{AOA,1}^2, \sigma_{AOA,2}^2, \ldots, \sigma_{AOA,L}^2 \right),$$

$$\frac{\partial \boldsymbol{f}_{AOA}(\boldsymbol{\psi}_t)}{\partial \boldsymbol{\psi}_t} = -\begin{bmatrix} \frac{y_t - y_1}{(x_t - x_1)^2 + (y_t - y_1)^2} & \frac{x_t - x_1}{(x_t - x_1)^2 + (y_t - y_1)^2} \\ \frac{y_t - y_2}{(x_t - x_2)^2 + (y_t - y_2)^2} & \frac{x_t - x_2}{(x_t - x_2)^2 + (y_t - y_2)^2} \\ \vdots & \vdots \\ \frac{y_t - y_L}{(x_t - x_L)^2 + (y_t - y_L)^2} & \frac{x_t - x_L}{(x_t - x_L)^2 + (y_t - y_L)^2} \end{bmatrix}. \quad (21)$$

Remark 4: In contrast to the AOA-based CRLB, the FIM of TOA-based localization can be represented by angular information θ_i as [18]

$$\boldsymbol{I}_{TOA}(\boldsymbol{\psi}_t) = \begin{bmatrix} \sum_{i=1}^{L} \frac{(x_t - x_i)^2}{r_i^2 \cdot \sigma_{TOA,i}^2} & \sum_{i=1}^{L} \frac{(x_t - x_i)(y_t - y_i)}{r_i^2 \cdot \sigma_{TOA,i}^2} \\ \sum_{i=1}^{L} \frac{(x_t - x_i)(y_t - y_i)}{r_i^2 \cdot \sigma_{TOA,i}^2} & \sum_{i=1}^{L} \frac{(y_t - y_i)^2}{r_i^2 \cdot \sigma_{TOA,i}^2} \end{bmatrix}$$
$$= \begin{bmatrix} \sum_{i=1}^{L} \frac{\cos^2\theta_i}{\sigma_{TOA,i}^2} & \sum_{i=1}^{L} \frac{\sin\theta_i \cos\theta_i}{\sigma_{TOA,i}^2} \\ \sum_{i=1}^{L} \frac{\sin\theta_i \cos\theta_i}{\sigma_{TOA,i}^2} & \sum_{i=1}^{L} \frac{\sin^2\theta_i}{\sigma_{TOA,i}^2} \end{bmatrix}. \quad (22)$$

However, the AOA-based CRLB cannot be simplified as (22) because the sufficient statistics of (21) requires both x and y coordinates. In order to resolve this issue, [19] used the u-statistics to compute the joint distribution of AOA-based CRLB. However, this method is accurate only when the number of participating anchors is sufficiently large.

To evaluate the average localization performance, we assume σ_{AOA} to be known and identical for each anchor [18], [19]

$$\sigma_{AOA} \triangleq \sigma_{AOA,1} = \sigma_{AOA,2} = \cdots = \sigma_{AOA,L}. \quad (23)$$

Then, the standard deviation of AOA measurement is computed as [16], [33]

$$\sigma_{AOA} = \sqrt{\frac{\mathbb{E}(r)^2}{10^{\mathbb{E}(SNR)/10}}}, \quad \text{where } \mathbb{E}(SNR) = \frac{\mathbb{E}[G]P_t}{N_0\, W_{TOT}}, \quad (24)$$

$\mathbb{E}(r)$ is the mean distance from all participating anchors, $\mathbb{E}(SNR)$ is the average signal-to-noise-ratio (SNR) for the mmWave network, $\mathbb{E}[G]$ is the mean channel gain, N_0 is the spectral density of the white Gaussian noise, and W_{TOT} is the total system bandwidth.

Remark 5: The assumption in (23) has been validated and justified in [14], [18], [19]. In this paper, we attempt to compute the average localization error using the AOA-based positioning, thus we assume that the AOA measurement is statistically independent with its means and same variance.

By using $\boldsymbol{I}_{AOA}(\boldsymbol{\psi}_t)$ in (20), the CRLB of AOA-based localization can be expressed as [18], [19]

$$CRLB = tr\left(\boldsymbol{I}_{AOA}^{-1}(\boldsymbol{\psi}_t)\right) = \frac{L \cdot \hat{\sigma}_{AOA}^2}{Q_1 - Q_2}, \tag{25}$$

where $\hat{\sigma}_{AOA}^2$ is the approximated AOA variance; Q_1 and Q_2 are given by

$$Q_1 = \sum_{i=1}^{L} \frac{(y_i - y_t)^2}{r_i^4} \cdot \sum_{j=1}^{L} \frac{(x_j - x_t)^2}{r_j^4},$$
$$Q_2 = \sum_{i=1}^{L} \frac{(x_i - x_t)^2 (y_i - y_t)^2}{r_i^8}. \tag{26}$$

In order to characterize the distribution of the CRLB in (25), (26) needs to be simplified. In the following Lemma, we use asymptotic bounds to approximate Q_1 and Q_2, which enable us to represent the AOA-based CRLB using a single variable.

Lemma 2: Q_1 and Q_2 in (26) can be approximated as

$$Q_1 \approx \left(\frac{1}{2}\sum_{i=1}^{L} \frac{1}{r_i^2}\right)^2, \quad Q_2 = \sum_{i=1}^{L} \frac{1}{4r_i^4}. \tag{27}$$

Proof: See Appendix B. □

Based on Lemma 2, (25) can be expressed as

$$CRLB \approx \frac{4L \cdot \hat{\sigma}_{AOA}^2}{\left(\sum_{i=1}^{L} \frac{1}{r_i^2}\right)^2 - \sum_{i=1}^{L} \frac{1}{r_i^4}} = \frac{4L \cdot \hat{\sigma}_{AOA}^2}{\sum\limits_{\substack{i,j=1 \\ i \neq j}}^{L} \frac{1}{r_i^2 r_j^2}}. \tag{28}$$

In the following Proposition, we will further simplify (28).

Proposition 1: Let us assume that the link distances are sorted in an ascending order, i.e., $r_1 \leq r_2 \leq \cdots \leq r_L$. The term $Q_1 - Q_2$ can be approximated as

$$Q_1 - Q_2 \triangleq \sum_{\substack{i,j=1 \\ i \neq j}}^{L} \frac{1}{r_i^2 r_j^2} \approx \frac{L(L-1)}{r_{\lceil L/4 \rceil}^4}, \tag{29}$$

where L is the number of participating anchors and $r_{\lceil L/4 \rceil}$ is the $\lceil L/4 \rceil$-th link distance in the ordered set $R = [r_1, \ldots, r_L]$.

In the following subsections, we employ two methods to justify the approximation in (29), namely, mutual information and root-finding. Then in Section IV, we use Monte Carlo simulation to validate the accuracy of (29).

1) MUTUAL INFORMATION

To justify (29), we will approximate $D \triangleq Q_1 - Q_2$ by an optimized approximation of r_k, denoted as r_*, given by

$$D \approx \frac{L(L-1)}{r_*^4}, \tag{30}$$

where the term r_* minimizes the mean square error (MSE)

$$r_* = \min_{1 \leq k \leq L} \mathbb{E}\left[\left|D - \frac{L(L-1)}{r_k^4}\right|^2\right]. \tag{31}$$

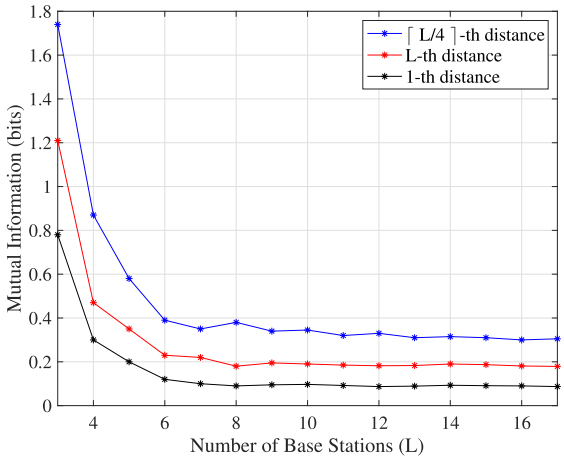

FIGURE 4. Impact of distance selection on mutual information.

Since R is a sorted set, the expression in (29) is bounded by

$$\frac{L(L-1)}{r_L^4} \leq \sum_{\substack{i,j=1 \\ i \neq j}}^{L} \frac{1}{r_i^2 r_j^2} \leq \frac{L(L-1)}{r_1^4}. \tag{32}$$

In [18], the authors introduced an approximation scheme where the best approximation was achieved by maximizing the mutual information. Furthermore, feature selection by maximizing the mutual information is a well know technique in machine learning and statistics [34]–[36]. Motivated by these approaches, we adopt a heuristic method and perform an iterative search to find the k-th term r_k, $1 \leq k \leq L$, as

$$\min_{1 \leq k \leq L} \mathbb{E}\left[\left|D - \frac{L(L-1)}{r_k^4}\right|^2\right] \Leftrightarrow \max_{1 \leq k \leq L} I(D; r_k|L), \tag{33}$$

where $I(D; r_k|L)$ is the mutual information (MI) between D and r_k for a given L. The MI is defined in terms of the differential entropies $h(D|L)$ and $h(D|r_k, L)$ as [18]

$$I(D; r_k|L) = h(D|L) - h(D|r_k, L), \tag{34}$$

where the supports of r_k and d are denoted by R_k and $\bar{D}$,

$$h(D|L) = -\sum_{d \in \bar{D}} f_D(d|L) \log_2 f_D(d|L),$$
$$h(D|r_k, L) = -\sum_{r_k \in R_k, d \in \bar{D}} f_{D;r_k}(d|r, L) \log_2 f_D(d|r, L). \tag{35}$$

Through extensive simulation, we observed that the $\lceil L/4 \rceil$-th distance achieves the maximum mutual information as illustrated in Fig. 4, thus we can use the $\lceil L/4 \rceil$-th distance to approximate D in (30), justifying Proposition 1. Furthermore, we observed that as the number of anchors increases, the mutual information trends to saturate for $L \geq 9$.

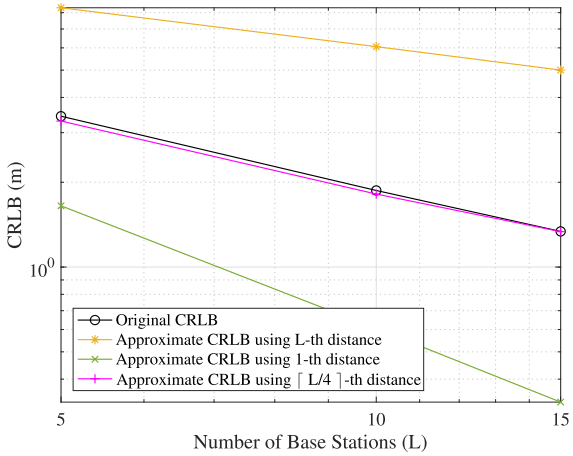

FIGURE 5. Original CRLB compared with approximate CRLBs.

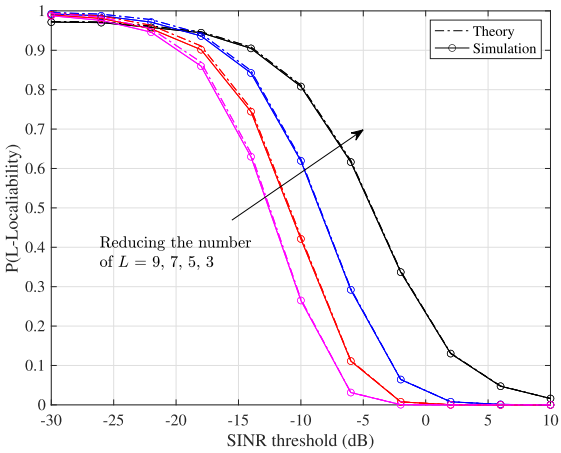

FIGURE 6. Impact of L on L-localizability when $\alpha_L = 2.1$, $\alpha_N = 4$, $L = 5$, $N_t = 64$ and $q = 0.75$.

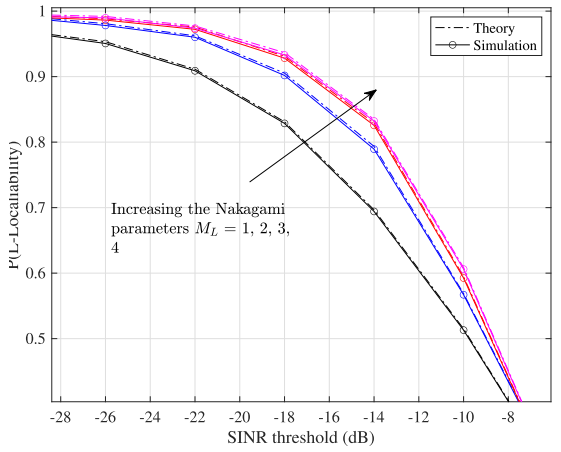

FIGURE 7. Impact of Nakagami fading parameter, M on L-localizability when $\alpha_L = 2.1$, $\alpha_N = 4$, $N_t = 64$ and $q = 0.75$.

2) ROOT-FINDING Method [37]

We may use root-finding algorithm as an alternative approach to approximate (29), where the optimized approximation of r_k is determined as the root of the following function

$$f(r) = \sum_{\substack{i,j=1 \\ i \neq j}}^{L} \frac{1}{r_i^2 r_j^2} - \frac{L(L-1)}{r^4}. \tag{36}$$

Since the range of r is bounded between $r_1 \leq r \leq r_L$ and (33), the following property holds; $f(r_L) \cdot f(r_1) < 0$. By applying Newton's iterative method, we found that the roots of (36) are located at the $\lceil \frac{5L}{16} \rceil$-th and $\lceil L/4 \rceil$-th distances, which validates (29) and Proposition 1.

Based on Proposition 1, the CRLB in (28) of the AOA-based localization can be approximated as follows

$$CRLB \approx \frac{4\,\hat{\sigma}_{AOA}^2}{L-1} \cdot r_{\lceil L/4 \rceil}^4. \tag{37}$$

We note that the CRLB in (37) is a function of $r_{\lceil L/4 \rceil}$, which is a random variable. In the following proposition, we provide the distribution of CRLB based on the distance distribution of $r_{\lceil L/4 \rceil}$ [27]. To remain consistency with the root mean square error, we derive the distribution of the squared-root CRLB, instead of CRLB.

Proposition 2: Let us assume that the number of participating anchors L and the standard deviation of AOA measurement σ_{AOA} are known. Based on [27], the CDF of a squared-root CRLB is given by

$$\begin{aligned} \mathrm{P}\left(\sqrt{CRLB} \leq s\right) &= F_{\sqrt{CRLB}}\left(s|L, \hat{\sigma}_{AOA}\right) \\ &= F_{r_{\lceil L/4 \rceil}}\left[\sqrt{\frac{s\sqrt{L-1}}{2\hat{\sigma}_{AOA}}}\middle| L, \hat{\sigma}_{AOA}\right], \end{aligned} \tag{38}$$

where $F_{r_n}(r)$ is the CDF of the n-th distance [27, eq. (9)].

Remark 6: In Fig. 5, we plot the CRLB curve evaluated by (25) (labeled as 'original CRLB'), (37) (labeled as '$\lceil L/4 \rceil$-th distance'), the 1-st and the L-th ordered distances. Note that there is a wide gap between the approximations of CRLB using the L-th, 1-st distance and the original CRLB. However, the approximation based on (37) accurately matches the exact CRLB, which justifies Proposition 1 and Proposition 2.

IV. SIMULATION RESULTS

In this section, we evaluate the L-localizability and AOA-based CRLB for mmWave networks, compare simulation results to numerical results, and investigate the impact of network parameters on the localization performance. We used MATLAB to simulate a realization of the node deployment 10^6 times. We assumed that the anchors are randomly distributed by a HPPP with density $\lambda = 2/\sqrt{3} \times 500^2 m^2$, bandwidth $W_{TOT} = 1$ GHz, transmit power $P_T = 1$ Watt, antenna spacing $d = \lambda_w/4$, path-loss intercept $\beta = (\lambda_w/4\pi)^2$, and antenna gain $G_1 = 1$ and $G_2 = 0.2$ with its associate probability $p_1 = 0.4$ and $p_2 = 0.6$, respectively.

In Figs. 6-7, we assessed the impact of network parameters on the performance of L-localizability. Specifically, we first

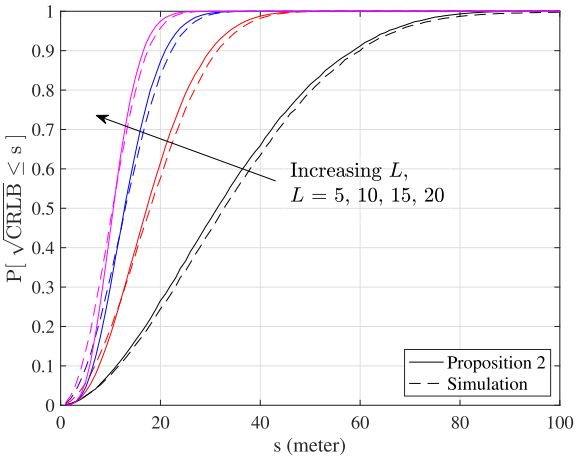

FIGURE 8. Impact of number of anchors on the distribution of $\sqrt{CRLB}$ when $\alpha_L = 2.1$, $N_t = 64$, $M_L = 5$ and $q = 0.75$.

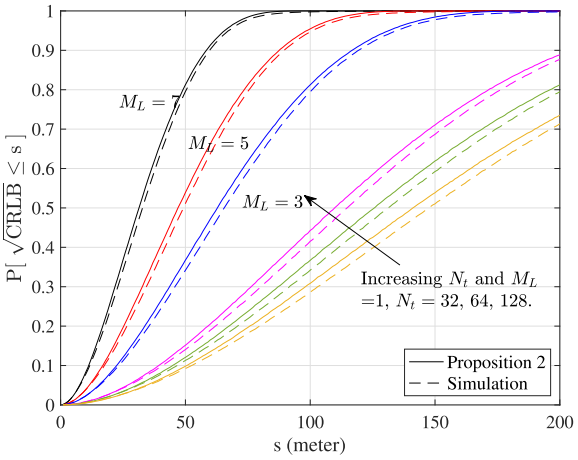

FIGURE 9. Impact of M ($M = 3, 5, 7$) on the distribution of $\sqrt{CRLB}$ when $\alpha_L = 2.1$, $N_t = 64$, $L = 5$, $q = 0.75$ and the impact of N_t ($N_t = 32, 64, 128$) when $\alpha_L = 2$, $M = 1$, $L = 5$ and $q = 0.75$.

plotted the L-localizability versus the SINR threshold across different number of participating anchors L in Fig. 6. Then we fixed L and compared the performance of L-localizability across different Nakagami fading parameter M_L in Fig. 7. The simulation results are plotted by circle markers with a line, whereas the analytical results are illustrated by dashed curves. We observed that the numerical results are very close to the analytical results, justifying the analysis. In Fig. 6, we note that reducing the number of participating anchors increases the L-localizability $P_L(\tau)$. This phenomenon is understandable as a large number of participating anchors leads to a higher interference, degrading the overall performance. In Fig. 7, we observed that the L-localizability performance escalates with a higher M_L value, which represents the Nakagami parameter of the LOS link. As M_L increases, the LOS channel becomes more deterministic while the NLOS channel condition remains fixed, which results in a higher SINR in (9) and better $P_L(\tau)$ in (10). Note that the case of $M_L = 1$ corresponds to Rayleigh fading environment.

In Figs. 8-9, we evaluated the distribution of the squared-root CRLB $\mathrm{P}(\sqrt{\mathrm{CRLB}} \leq s)$ and compared its performance across various configuration of network parameters. The numerical results are evaluated by using (38) in Proposition 2 and plotted by solid curves, whereas the simulation results are illustrated by dotted curves. We used the approximation based on the $\lceil L/4 \rceil$-th distance and observed that the numerical results closely match simulation results, validating the accuracy of Proposition 2. In Fig. 8, we observed that $\mathrm{P}(\sqrt{\mathrm{CRLB}} \leq s)$ is an increasing function of L, indicating that the localization error declines for a large number of participating anchors. Hence, a network designer looking to improve the localization accuracy needs to optimize the network environment to ensure a sufficient number of anchors participate in the localization procedure. For example, a joint optimization problem can be designed that maximizes the CRLB distribution $\mathrm{P}(\sqrt{\mathrm{CRLB}} \leq s)$ given that the L-localizability $P_L(\tau)$ is above certain threshold. Fig. 9 compares the localization performance for various Nakagami parameter M_L and the number of antenna elements N_t. We observed that increasing M_L parameter improves the localization performance, which provides similar result in Fig. 7. Furthermore, we consider the impact of the number of antenna N_t on the localization performance. For a larger N_t, the normalized noise power $\sigma_n^2 = \frac{\sigma_T^2}{\beta P_t N_t}$ will decrease, resulting in a higher $\mathrm{P}(\sqrt{\mathrm{CRLB}} \leq s)$. This indicates that the localization performance can be enhanced by adding more antenna elements in the anchors, which raises the implementation cost for each anchor.

V. CONCLUSION

This paper presents L-localizability and random AOA-based CRLB for mmWave wireless networks, where we used stochastic geometry to account for all possible positioning scenarios. We derived the L-localizability and random CRLB for AOA localization while considering the flat-top antenna radiation pattern and Nakagami fading. We provided numerical results to validate the analytical derivation and investigated the impact of various network parameters, *e.g.*, network load, fading parameters, number of anchors, number of antenna elements, on the localization performance. The analytical framework developed in this paper offers an accurate tool to evaluate the localization performance of mmWave wireless networks without relying on extensive simulation. The network operators can use the asymptotic bounds to optimize the network parameters and find the best deployment of the anchors to ensure localization performance.

APPENDIX A

The interference inside the LOS ball except for the nearest anchor is approximated as [14]:

$$\mathbb{E}\left[\hat{I}_1 | r_1, r_L, L\right] = \mathbb{E}[G_T] \cdot \int_{r_1}^{r_L} \int_0^{\infty} \frac{2r}{r_L^2 - r_1^2} r^{-\alpha_L} \cdot hf(h) dh dr$$

$$= \mathbb{E}[G_T] \cdot \mathbb{E}[h] \cdot \frac{2(\hat{L}-1)}{2-\alpha_L} \cdot \frac{r_L^{2-\alpha_L} - r_1^{2-\alpha_L}}{r_L^2 - r_1^2}, \quad (39)$$

where $f(h)$ is the PDF of the desired channel power, $\mathbb{E}[G_T] = G_1 p_1 + G_2 p_2$ and $\mathbb{E}[h]$ is the mean channel gain.

APPENDIX B

First, we derive the lower bound of Q_2 as follows

$$Q_2 \overset{(a)}{\geq} \sum_{i=1}^{L} \frac{\frac{1}{4}[(x_i - x_t)^2 + (y_i - y_t)^2]^2}{r_i^8} \overset{(b)}{=} \sum_{i=1}^{L} \frac{1}{4r_i^4}, \quad (40)$$

where the inequality $(x_i - x_t)^2 + (y_i - y_t)^2 \geq 2(x_i - x_t)(y_i - y_t)$ is applied to step (a) and Cartesian coordinates is converted to polar coordinate in step (b). As the polar coordinate of (x_i, y_i) is given by

$$x_i - x_t = r_i \cos(\theta_i), \quad y_i - y_t = r_i \sin(\theta_i), \quad (41)$$

we derive the upper bound of Q_1 as

$$\begin{aligned} Q_1 &= \sum_{i=1}^{L} \frac{(y_i - y_t)^2}{r_i^4} \sum_{j=1}^{L} \frac{(x_j - x_t)^2}{r_j^4} \\ &= \sum_{i=1}^{L} \frac{\sin^2(\theta_i)}{r_i^2} \sum_{j=1}^{L} \frac{\cos^2(\theta_j)}{r_j^2}, \end{aligned} \quad (42)$$

where we will maximize Q_1 with respect to the phase $\{\theta_i\}$ for a given distance $\{\theta_i\}$. Then, (42) can be expressed as

$$Q_1 = \sum_{i=1}^{L} \frac{\sin^2(\theta_i)}{r_i^2} \sum_{j=1}^{L} \frac{1 - \sin^2(\theta_j)}{r_j} = \xi \left(\sum_{j=1}^{L} \frac{1}{r_j^2} - \xi \right), \quad (43)$$

where we denote $\xi \triangleq \sum_{i=1}^{L} \frac{\sin^2(\theta_i)}{r_i^2}$. The first order derivative of Q_1 is zero when $\xi^* = \frac{1}{2} \sum_{i=1}^{L} \frac{1}{r_i^2}$ and the second order derivative of Q_1 has a negative value at ξ^* as follows

$$\begin{aligned} \frac{\partial Q_1}{\partial \xi} &= \sum_{i=1}^{L} \frac{1}{r_i^2} - 2\xi = 0 \Rightarrow \xi^* = \frac{1}{2} \sum_{i=1}^{L} \frac{1}{r_i^2}, \\ \frac{\partial^2 Q_1}{\partial \xi^2} &= -2 < 0. \end{aligned} \quad (44)$$

Thus, Q_1 is upper bounded by

$$Q_1 \leq \max_{\{\theta_i\}} Q_1 \Big|_{\xi = \xi^*} = \left(\frac{1}{2} \sum_{i=1}^{L} \frac{1}{r_i^2} \right)^2. \quad (45)$$

This completes the proof.

REFERENCES

[1] F. Khelifi, A. Bradai, A. Benslimane, P. Rawat, and M. Atri, "A survey of localization systems in Internet of Things," *Mobile Netw. Appl.*, vol. 24, no. 3, pp. 761–785, Jun. 2019.

[2] M. D. Dikaiakos, A. Florides, T. Nadeem, and L. Iftode, "Location-aware services over vehicular ad-hoc networks using car-to-car communication," *IEEE J. Sel. Areas Commun.*, vol. 25, no. 8, pp. 1590–1602, Oct. 2007.

[3] F. Wen, J. Kulmer, K. Witrisal, and H. Wymeersch, "5G positioning and mapping with diffuse multipath," *IEEE Trans. Wireless Commun.*, vol. 20, no. 2, pp. 1164–1174, Feb. 2021.

[4] M. Wang, F. Gao, S. Jin, and H. Lin, "An overview of enhanced massive MIMO with array signal processing techniques," *IEEE J. Sel. Topics Signal Process.*, vol. 13, no. 5, pp. 886–901, Sep. 2019.

[5] A. Alkhateeb, S. Alex, P. Varkey, Y. Li, Q. Qu, and D. Tujkovic, "Deep learning coordinated beamforming for highly-mobile millimeter wave systems," *IEEE Access*, vol. 6, pp. 37328–37348, 2018.

[6] Y. Ge, H. Kim, F. Wen, L. Svensson, S. Kim, and H. Wymeersch, "Exploiting diffuse multipath in 5G SLAM," in *Proc. GLOBECOM-IEEE Global Commun. Conf.*, Taipei, Taiwan, Dec. 2020, pp. 1–6.

[7] D. Wang, M. Fattouche, and X. Zhan, "Pursuance of mm-level accuracy: Ranging and positioning in mmWave systems," *IEEE Syst. J.*, vol. 13, no. 2, pp. 1169–1180, Jun. 2019.

[8] F. Lemic , J. Martin, C. Yarp, D. Chan, V. Handziski, R. Brodersen, A. Wolisz, J. Wawrzynek "Localization as a feature of mmWave communication," in *Proc. Int. Wireless Commun. Mobile Comput. Conf. (IWCMC)*, Paphos, Cyprus, Sep. 2016, pp. 1033–1038.

[9] H. C. So, "Source localization: Algorithms and analysis," in *Handbook of Position Location: Theory, Practice and Advances*, S. A. Zekavat and M. Buehrer, Eds. Hoboken, NJ, USA: Wiley, 2019, ch. 3.

[10] Z. Abu-Shaban, H. Wymeersch, T. D. Abhayapala, and G. Seco-Granados, "Single-anchor two-way localization bounds for 5G mmWave systems," *IEEE Trans. Veh. Technol.*, vol. 69, no. 6, pp. 6388–6400, Jun. 2020.

[11] M. Pajovic, P. Wang, T. Koike-Akino, H. Sun, and P. V. Orlik, "Fingerprinting-based indoor localization with commercial mmWave WiFi—Part I: RSS and beam indices," in *Proc. IEEE Global Commun. Conf. (GLOBECOM)*, Waikoloa, HI, USA, Dec. 2019, pp. 1–6.

[12] R. Mendrzik, H. Wymeersch, G. Bauch, and Z. Abu-Shaban, "Harnessing NLOS components for position and orientation estimation in 5G millimeter wave MIMO," *IEEE Trans. Wireless Commun.*, vol. 18, no. 1, pp. 93–107, Jan. 2019.

[13] J. Yang, S. Jin, C.-K. Wen, J. Guo, M. Matthaiou, and B. Gao, "Model-based learning network for 3-D localization in mmWave communications," *IEEE Trans. Wireless Commun.*, vol. 20, no. 8, pp. 5449–5466, Aug. 2021.

[14] J. Schloemann, H. S. Dhillon, and R. M. Buehrer, "Toward a tractable analysis of localization fundamentals in cellular networks," *IEEE Trans. Wireless Commun.*, vol. 15, no. 3, pp. 1768–1782, Mar. 2016.

[15] C. E. O'Lone, H. S. Dhillon, and R. M. Buehrer, "Single-anchor localizability in 5G millimeter wave networks," *IEEE Wireless Commun. Lett.*, vol. 9, no. 1, pp. 65–69, Jan. 2020.

[16] R. Koirala, B. Denis, D. Dardari, and B. Uguen, "Localization bound based beamforming optimization for multicarrier mmWave MIMO," in *Proc. 14th Workshop Positioning, Navigat. Commun. (WPNC)*, Bremen, Germany, Oct. 2017, pp. 1–6.

[17] D. Wang, M. Fattouche, and F. M. Ghannouchi, "Bounds of mmWave-based ranging and positioning in multipath channels," in *Proc. IEEE Globecom Workshops (GC Wkshps)*, Singapore, Dec. 2017, pp. 1–6.

[18] C. E. O'Lone, H. S. Dhillon, and R. M. Buehrer, "A statistical characterization of localization performance in wireless networks," *IEEE Trans. Wireless Commun.*, vol. 17, no. 9, pp. 5841–5856, Sep. 2018.

[19] B. Huang, T. Li, B. D. O. Anderson, and C. Yu, "On the performance limit of sensor localization," in *Proc. IEEE Conf. Decis. Control Eur. Control Conf.*, Orlando, FL, USA, Dec. 2011, pp. 7870–7875.

[20] M. Haenggi, *Stochastic Geometry for Wireless Networks*. Cambridge, U.K.: Cambridge Univ. Press, 2013.

[21] D. Puccinelli and M. Haenggi, "Wireless sensor networks: Applications and challenges of ubiquitous sensing," *IEEE Circuits Syst. Mag.*, vol. 5, no. 3, pp. 19–31, Sep. 2005.

[22] R. K. Ganti and M. Haenggi, "Interference and outage in clustered wireless ad hoc networks," *IEEE Trans. Inf. Theory*, vol. 55, no. 9, pp. 4067–4086, Sep. 2009.

[23] M. R. Akdeniz , Y. Liu, M. K. Samimi, S. Sun, S. Rangan, T. S. Rappaport, E. Erkip, "Millimeter wave channel modeling and cellular capacity evaluation," *IEEE J. Sel. Areas Commun.*, vol. 32, no. 6, pp. 1164–1179, Jun. 2014.

[24] T. Bai and R. W. Heath, "Coverage in dense millimeter wave cellular networks," in *Proc. Asilomar Conf. Signals, Syst. Comput.*, Pacific Grove, CA, USA, Nov. 2013, pp. 2062–2066.

[25] T. Bai, A. Alkhateeb, and R. W. Heath, "Coverage and capacity of millimeter-wave cellular networks," *IEEE Commun. Mag.*, vol. 52, no. 9, pp. 70–77, Sep. 2014.
[26] T. Bai and R. W. Heath, Jr., "Coverage and rate analysis for millimeter-wave cellular networks," *IEEE Trans. Wireless Commun.*, vol. 14, no. 2, pp. 1100–1114, Feb. 2015.
[27] S. Srinivasa and M. Haenggi, "Distance distributions in finite uniformly random networks: Theory and applications," *IEEE Trans. Veh. Technol.*, vol. 59, no. 2, pp. 940–949, Feb. 2010.
[28] D. Moltchanov, "Distance distributions in random networks," *Ad Hoc Netw.*, vol. 10, no. 6, pp. 1146–1166, 2012.
[29] J. G. Andrews, T. Bai, M. N. Kulkarni, A. Alkhateeb, A. K. Gupta, and R. W. Heath, Jr., "Modeling and analyzing millimeter wave cellular systems," *IEEE Trans. Commun.*, vol. 65, no. 1, pp. 403–430, Jan. 2017.
[30] G. Lee, Y. Sung, and M. Kountouris, "On the performance of random beamforming in sparse millimeter wave channels," *IEEE J. Sel. Topics Signal Process.*, vol. 10, no. 3, pp. 560–575, Apr. 2016.
[31] X. Yu, J. Zhang, M. Haenggi, and K. B. Letaief, "Coverage analysis for millimeter wave networks: The impact of directional antenna arrays," *IEEE J. Sel. Areas Commun.*, vol. 35, no. 7, pp. 1498–1512, Jul. 2017.
[32] H. Alzer, "On some inequalities for the incomplete gamma function," *Math. Comput.*, vol. 66, pp. 771–778, Apr. 1997.
[33] M. Giordani, M. Mezzavilla, A. Dhananjay, S. Rangan, and M. Zorzi, "Channel dynamics and SNR tracking in millimeter wave cellular systems," in *Proc. 22th Eur. Wireless Conf.*, Oulu, Finland, 2016, pp. 1–8.
[34] P. A. Estévez, M. Tesmer, C. A. Perez, and J. M. Zurada, "Normalized mutual information feature selection," *IEEE Trans. Neural Netw.*, vol. 20, no. 2, pp. 189–201, Feb. 2009.
[35] Y. Lin, Q. Hu, J. Liu, J. Li, and X. Wu, "Streaming feature selection for multilabel learning based on fuzzy mutual information," *IEEE Trans. Fuzzy Syst.*, vol. 25, no. 6, pp. 1491–1507, Dec. 2017.
[36] J. Wang, J. Wei, Z. Yang, and S. Wang, "Feature selection by maximizing independent classification information," *IEEE Trans. Knowl. Data Eng.*, vol. 29, no. 4, pp. 828–841, Apr. 2017.
[37] R. Pasupathy, "On choosing parameters in retrospective-approximation algorithms for stochastic root finding and simulation optimization," *Oper. Res.*, vol. 58, pp. 889–901, Aug. 2010.

JIAJUN HE (Student Member, IEEE) was born in Guangzhou, China. He received the master's degree in source localization using wireless techniques from the City University of Hong Kong, in 2018, where he is currently pursuing the Ph.D. degree mainly researching wireless communication with an emphasis on stochastic geometry. His research interests include source localization, mobile edge computing, wireless communications, and deep learning.

YOUNG JIN CHUN (Member, IEEE) received the B.S. degree in electrical engineering from Yonsei University, in 2004, the M.S. degree in electrical engineering from the University of Michigan, in 2007, and the Ph.D. degree in electrical engineering from Iowa State University, in 2011. From September 2011 to October 2018, he had been with Sungkyunkwan University, Qatar University, and Queen's University Belfast, on various academic positions. He joined the Department of Electronic Engineering, City University of Hong Kong, as an Assistant Professor of wireless communication, in November 2018. His research interests include wireless communications with an emphasis on stochastic geometry, system-level network analysis, device-to-device communications, and various use-cases of 5G communications.